Polymer Journal, Vol. 32, No. 4, pp 339—347 (2000)

Poly(phenylene sulfide) and Low-Density Polyethylene Reactive Blends. Morphology, Tribology, and Moldability

Shin HORIUCHI and Yoshiaki ISHII*

Department of Polymer Engineering, National Institute of Materials and Chemical Research, 1-1 Higashi, Tsukuba, Ibaraki 305-8565, Japan
**Otsuka Chemical Co., Ltd., 463 Kagasuno, Kawakami, Tokushima 771-0193, Japan*

(Received July 28, 1999)

ABSTRACT: Morphology, tribology, and moldability of poly(phenylene sulfide) (PPS) and low density polyethylene (LDPE) reactive blends were investigated. Tribological properties (friction and wear) are synergistically improved in the blends of PPS/LDPE (90/10 by weight). However, the simple blending of PPS/LDPE give rise to the deposition on the mold surface in the cyclic operation of injection molding, which causes poor surface appearance of mold articles and leads to poor productivity. Glycidyl functional materials work as coupling agents between the PPS matrix and the domains of LDPE grafted with maleic anhydride (LDPEgMA) during melt mixing, resulting in the reduction of the domain size. It was found that introduction of the coupling reaction between PPS and LDPEgMA prevents the "mold deposition" (MD), whereas the good tribological properties are maintained. Furthermore, notched izod impact strength is increased, and then, specific balanced combination of physical and thermal properties can be achieved. Morphological analysis was performed by electron spectroscopic imaging (ESI) and electron energy loss spectroscopy (EELS) on an energy-filtering transmission electron microscope (EFTEM). It was revealed that the LDPE domains are not encapsulated by the glycidyl functional materials, but those two phases are stuck together. It was concluded that the preferable properties were achieved owing to the synchronization of the each three phase, *i.e.*, PPS, LDPE, and the glycidyl functional material's phases, by taking the "stuck phase formation".

KEY WORDS Poly(phenylene sulfide) / Low-Density Polyethylene / Reactive Blend / Morphology / Tribology / Moldability / Energy-Filtering Transmission Electron Microscope /

Reactive polymer blending has been recognized as the useful way to develop high performance polymer materials. It is effective to achieve fine dispersion of the polymers in immiscible binary polymer blends, and also to attain sufficient interfacial adhesion between the matrix and dispersed phases. The reactive blending was also employed in poly(phenylene sulfide) (PPS) based blends. The objective of the PPS based reactive blends is mainly for the improvement of its brittleness by incorporating olefinic elastomers grafted with maleic anhydride (MA). The most such works, however, appear in patent literatures[1—3] and very few scientific works have been reported.[4—8] PPS has simple repeating units synthesized by condensation polymerization from sodium sulfide (Na_2S) and *p*-dichlorobenzene,[9] hence, there seems to be no possibility for reactions. The previous works suggested the reactivity of PPS against glycidyl or isocyanate functional groups, however, the detail reaction manner has been unknown.

PPS is a semicrystalline high performance thermoplastic with outstanding thermal and chemical durability. The neat PPS resin, however, has been rarely used because of its brittleness, and usually it is filled with inorganic fillers to overcome its demerits. On the other hand, PPS has been blended with other polymers, such as polysulfones, polyarylates, polyamides, fluoropolymers, and liquid crystal polymers, and some grades have been commercially established to offer materials with specific balanced combination of physical properties.[10]

We here report the morphology, tribology, and moldability of the ternary reactive blends of PPS, low-density polyethylene grafted with maleic anhydride (LDPEgMA), and a glycidyl functionalized material that is expected to work as a coupling agent between PPS and LDPEgMA. Detail morphological characterizations were performed by electron spectroscopic imaging (ESI) and electron energy loss spectroscopy (EELS) on an energy-filtering transmission electron microscope (EFTEM). EFTEM is one of the analytical electron microscopes, which allows us to analyze local element compositions by EELS and to create element-specific images by ESI. ESI offers element distribution images with the aid of image processing techniques, which are called two-window or three window methods, to extrapolate the background signals from corresponded element-specific electron spectroscopic images. It has been recognized that EFTEM has great advantage in terms of the nano-scale local analysis, especially, for light elements, such as carbon, nitrogen, and oxygen. We demonstrated the application of EFTEM to the morphological analysis of polymer blends[11] and to the analysis of immiscible polymer–polymer interfaces.[12] Here, we apply ESI and EELS to the analysis of morphologies that are difficult to be characterized by the conventional staining techniques.

Tribological properties (friction and wear) have been recognized to be of considerable importance for industrial applications of engineering plastics in a dynamic contact environment, particularly, for use as a substitute for metal. Also, self-lubricating materials with low friction coefficient and with high wear resistance are desired in the point of economical and ecological views.

Furthermore, we evaluated the moldability of the blends in the cyclic operation of injection molding by inspecting the occurrence of "mold deposition" (MD). The MD would cause poor surface appearance of molded articles and poor productivity. Prevention of MD is essential for plastics to be used practically for molding materials.

Table I. Materials used in this study

Polymer (Designation)	Composition	Molecular weight	Product name (Source)
Poly(phenylene sulfide) (PPS)		M_w : 260000	Rayton L2120 (Toray Co.)
MA grafted low density polyethylene (LDPEgMA)	MA content : 0.1 wt%	M_w : 110000 M_n : 29000	Adtechs L6100M (Japan Polyolefine Co.)
Ethylene-glycidyl methacrylate copolymer (PE-GMA)	GMA content : 12 wt%	M_w : 200000 M_n : 35000	BondfastE-GMA (Sumitomo Chem. Co.)
Ethylene-methylmethacrylate copolymer (PE-MMA)	MMA content : 10 wt%		Acryft WD301 (Sumitomo Chem. Co.)
Diglycidyl ether of bisphenol A (DGEBA)	Epoxy equivalent : 900—1000 g/eq.	M_n : 1800—2000	EPOTOHTO YD-014 (Tohto Chem. Co.)

EXPERIMENTAL

Materials

The materials used in this study are listed in Table I. A random copolymer of ethylene and glycidyl methacrylate (PE-GMA) and a solid di-functional epoxy resin (diglycidyl ether bisphenol A, DGEBA) are expected to react to both PPS and LDPEgMA, working as coupling agents. To evaluate the reactivity of PPS against glycidyl functional groups, a random copolymer of ethylene and methyl methacrylate (PE-MMA) was also used, which has a similar main chain structure as PE-GMA and has different side chain groups with no reactivity. Through a comparative study between the blends with PE-GMA and with PE-MMA, we could discuss the effect of the glycidyl functional groups on the morphologies and the properties.

Processing

All blends were prepared on a co-rotating 50 mm twin-screw extruder ($L=1750$ mm, $L/D=35$; TEX44, Japan Steel Works, Ltd.). The rotating speed of screw was at 100 rpm, the feeding rate was 333 g min^{-1}, and the barrel temperature was set between 230 and 300℃ as shown in Figure 1. For the preparation of ternary blends, the two components except LDPEgMA were firstly fed from the main hopper at zone 1, and then LDPEgMA was fed from the side hopper at zone 5. The blends thus prepared were injection-molded by an injection molding machine (M26/15B, Sumitomo Heavy Industries, Ltd.) at the barrel temperatures between 230 and 310, and at the mold temperature of 120℃. The mold surface was inspected in terms of the occurrence of the MD under a magnifier after certain cycles of the injection molding.

Morphology

Morphological characterization was carried out on a transmission electron microscope (TEM). An EFTEM, Carl Ziess EM902, was used at an acceleration voltage of 80 kv. Thin sections from the injection molded specimens were cut on an ultramicrotome (Reichert UltracutE) under a cryogenic condition at −105℃ with a diamond knife. Conventional TEM observation was carried out with specimens stained with RuO_4. The statistical analysis regarding the dispersion of LDPE domains were performed by digital image analysis on an IBAS

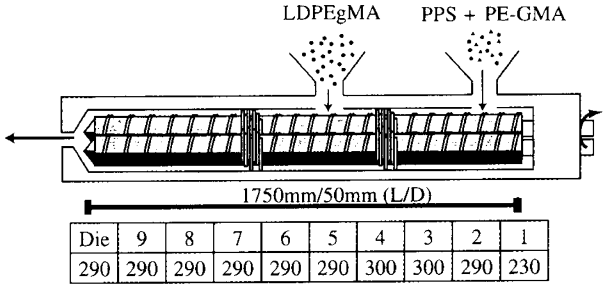

Figure 1. Mixing condition and the configuration of the twin screw extruder used in this study.

image processor.

For detail characterization of the phase formations of the blends, ESI and EELS were employed with unstained specimens. By ESI mode, carbon, oxygen and sulphur distribution images were created by "three window power law method" :[13] Three electron spectroscopic images (ES-images) at different energy loss levels were recorded on "Imaging Plates" (IP's), two of which are formed by electrons below the edge of the core loss peak of a certain element, and the other of which is formed by electron at the core loss peak. The background image is created using the two pre-edge images by an intra-image calculation with the eq 1,

$$I(E)=AE^{-r} \tag{1}$$

where I is the signal intensity, E is the loss energy, and the factors A and r are calculated pixel by pixel. And then, an element distribution image is obtained by subtraction of the background image from the core loss image.

An electron energy loss spectrum (EEL-spectrum) from a slected region on a specimen was obtained by "parallel recording"[14] on an IP : A spectrum from a local region selected by inserting an aperture in a selective energy loss level was recorded on an IP, and the intensity profile was read out by a IP processing system, FLD 5000 (Fuji Photo Film Co. Ltd.). Energy losses in the width of about 120 eV can be simultaneously recorded on a single IP.

Tribology

Tribological tests were performed on a Suzuki-type friction machine in accordance with JIS J7218. A cylindrical specimen with a contact area of 2 cm^2 prepared by injection molding was slid against a stainless steel (S45

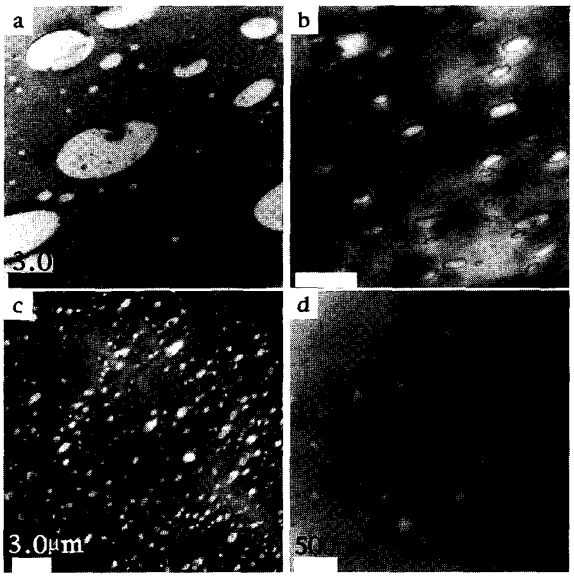

Figure 2. TEM photographs of the binary blends (90/10) of (a) PPS/LDPEgMA, (b) PPS/PE-GMA, (c) PPS/PE-MMA, and (d) PPS/DGEBA. The specimens were stained with RuO_4.

Table II. Average and maximum domain sizes obtained from the TEM photographs

Formulation		Domain Size/μm	
by weight		Average	Maximum
PPS/LDPEgMA	90/10	1.10	8.36
PPS/PE-GMA	90/10	0.30	1.19
PPS/PE-MMA	90/10	0.47	3.07
PPS/DGEBA	90/10	0.22	0.43
PPS/LDPE/E-GMA	89/10/1	0.96	4.95
	87/10/3	0.62	1.56
	85/10/5	0.57	1.93
PPS/LDPE/E-MMA	89/10/1	1.46	9.32
	87/10/3	1.46	7.15
	85/10/5	1.59	7.27
PPS/LDPE/Epoxy	89/10/1	0.79	7.52
	87/10/3	0.54	1.36
	85/10/5	0.47	1.30

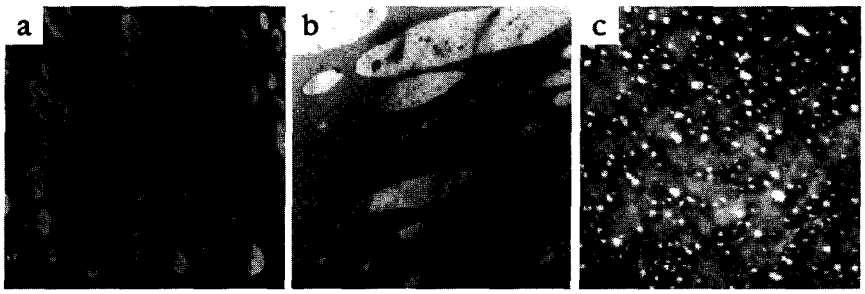

Figure 3. TEM photographs of the ternary blends (85/10/5) of (a) PPS/LDPEgMA/PE-GMA, (b) PPS/LDPEgMA/PE-MMA, and (c) PPS/LDPEgMA/DGEBA. The specimens were stained with RuO_4.

C) cylinder with the same configuration under a load of 196 N and at a speed of 0.3 m s^{-1}. The coefficient of friction and the specific wear rate were obtained after the sliding distance reached to 10 km.

Mechanical Properties

Notched izod impact strengths were measured at an ambient condition according to ASTM D 256. Tensile and flexural characteristics were also investigated at an ambient condition by following the ASTM D638 and ASTM D790, respectively. Heat deflection temperature (HDT) at which an injection molded bar (5×0.5×0.25 inch) deflects 0.010 inch under a load of 18.2 MPa was measured in accordance with ASTM D 648.

Thermal Analysis

For the characterization of the crystallization behaviors, differential scanning calorimetry (DSC) was performed using a SSC5200 (Seiko Instruments Co. Ltd.). The samples were heated from 30 to 200℃ at the rate of 5 K min^{-1}.

RESULTS AND DISCUSSION

Morphology

Firstly, the morphologies of the binary blends of PPS/LDPEgMA, PPS/PE-GMA, PPS/PE-MMA, and PPS/DGEBA (90/10) are shown in Figure 2. The average and maximum domain sizes obtained from those TEM photographs are summarized in Table II. The binary blend of PPS/LDPEgMA exhibits poor dispersion of LDPE domains, the size distribution is broad, and extremely large domains exist. The binary blends of PPS/PE-GMA, PPS/PE-MMA and DGEBA, on the other hand, shows finer dispersion and narrower size distribution than that of the PPS/LDPEgMA binary blend. Especially, the blends with the glycidyl functional materials, *i.e.*, PE-GMA and DGEBA, show much finer and narrower dispersion. These results suggest that the glycidyl functional groups can react to PPS.

Figure 3 shows the TEM photographs of the ternary blends of PPS/LDPEgMA/PE-GMA, PPS/LDPEgMA/PE-MMA, and PPS/LDPEgMA/DGEBA (85/10/5). These photographs clearly indicate that the additions of the glycidyl functional materials effectively reduce the LDPE domain size, whereas PE-MMA has no effect on the reduction of the LDPE domain size. Figure 4 shows the average and the maximum domain sizes as a function of the content of PE-GMA, PE-MMA, and DGEBA, where the LDPEgMA content is fixed at 10 wt% and the contents of PE-GMA, PE-MMA and DGEBA are varied from 1 to 5 wt%. The average domain size is reduced as

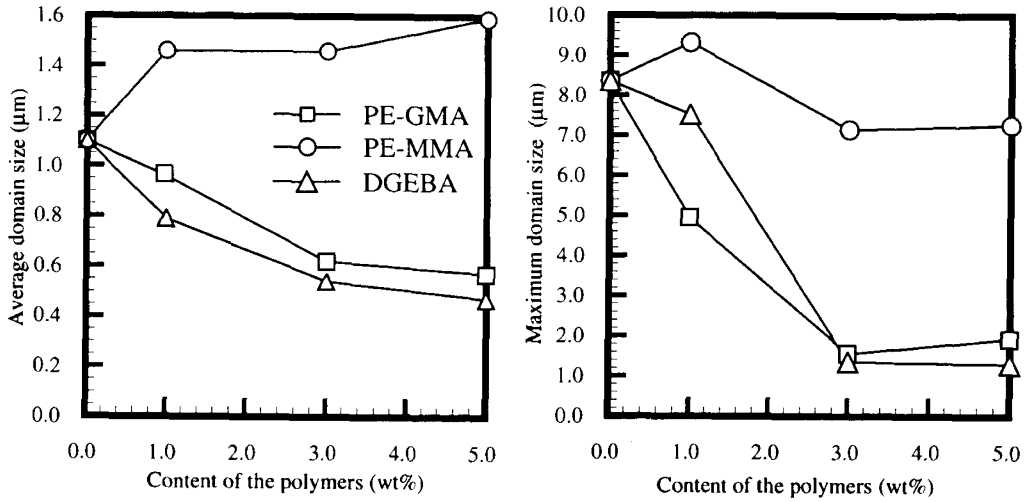

Figure 4. The average and the maximum LDPE domain sizes as a function of the content of PE-GMA (□), PE-MMA (○), and DGEBA (△). The LDPEgMA content is fixed at 10 wt%, and the content of those three materials are varied from 1 to 5 wt%.

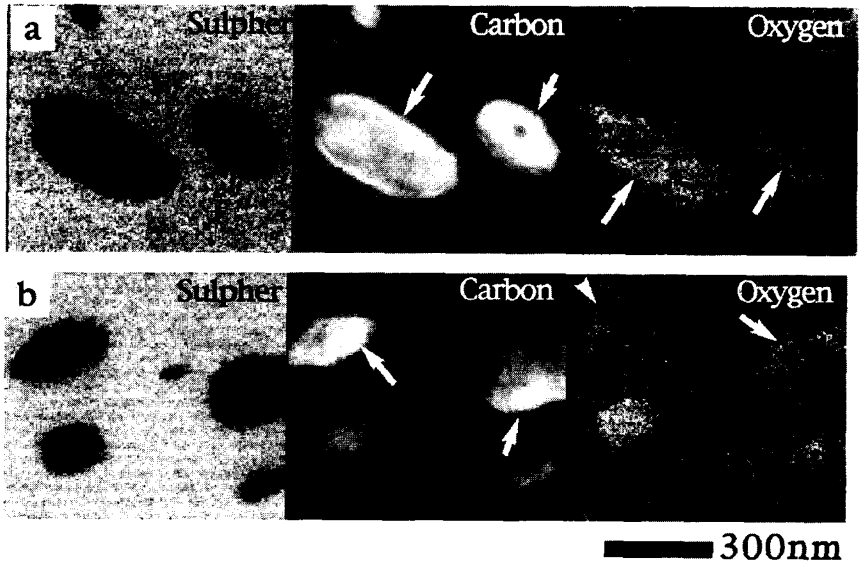

Figure 5. Sulphur, carbon, and oxygen distribution images created by "three window power law method" of ternary reactive blends. (a) is PPS/LDPEgMA/PE-GMA (85/10/5) and (b) is PPS/LDPEgMA/DGEBA (85/10/5).

an increase of the amount of PE-GMA and DGEBA. By the addition of 5 wt% of those materials, the average size decreases to about one-third of the binary blend of PPS/LDPE (90/10). Notably, the maximum domain size is drastically decreased by the addition of these materials as shown in Figure 4b. This means that the dispersion of the LDPE domains in the PPS matrix become fine and uniform by the addition of PE-GMA or DGEBA. On the other hand, PE-MMA cannot improve the dispersion of the LDPE domain at all.

Above all results strongly suggest that PPS has reactivity against glycidyl functional materials, and that PE-GMA and DGEBA work as coupling agents between PPS and LDPEgMA. Therefore, PE-GMA and DGEBA phases are assumed to be located at the interface between the PPS and the LDPE phases. However, conventional TEM observation cannot identify the location of these phases because RuO_4 stains PPS phase most strongly among the materials, and LDPEgMA, PE-GMA and PE-MMA phases are hardly distinguished because they have the similar chemical and crystalline structures. However, differences of elemental composition between LDPEgMA and PE-GMA, PE-MMA, and DGEBA are expected to distinguish between them by ESI and EELS. That is, the oxygen concentration of LDPEgMA is significantly low as compared to PE-GMA, PE-MMA, and DGEBA because the grafted maleic anhydride on LDPE is less than 0.1 wt%, and the carbon concentration of LDPEgMA is enough higher than those three materials to be distinguished from each other. Therefore, carbon and oxygen distribution images were created by ESI, and corresponding EEL-spectra from selected local regions were taken to discuss morphological aspects of the blend series deeply.

Figure 5 shows sulphur, carbon and oxygen distribution images of ternary blends of PPS/LDPEgMA/PE-GMA and PPS/LDPEgMA/DGEBA (85/10/5) created by "three window power law method". For sulphur distribu-

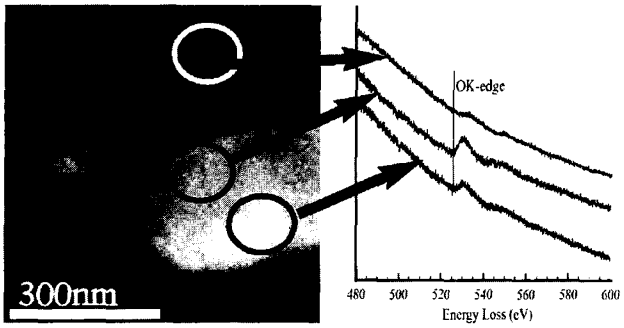

Figure 6. A carbon distribution image of the ternary blend of PPS/LDPEgMA/DGEBA and EEL-spectra showing O K-edges taken from the local area assigned in the image.

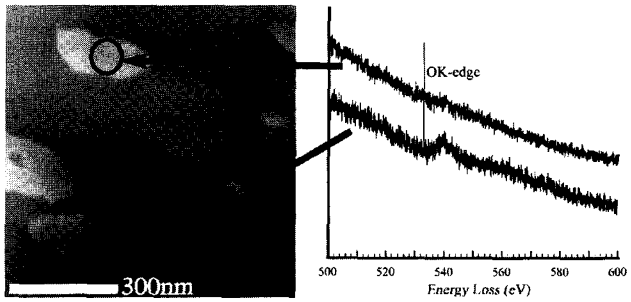

Figure 7. A zero-loss image of the ternary blend of PPS/LDPEgMA/PE-GMA (85/10/5) and EEL-spectra taken from the regions assigned in the image.

tion images, three ES-images formed by electrons with an energy loss of 132.5±7.5, 152.5±7.5, and 172.5±7.5 eV were used; for carbon distribution images, images with an energy loss of 247.5±7.5, 267.5±7.5, and 292.5 ±7.5 were used; and for oxygen distribution images, images with an energy loss of 502.5±7.5, 522.5±7.5, and 542.5±7.5 were used. The sulphur distribution images clearly exhibit the PPS matrix phase. The image contrast in the carbon distribution images reflects the relative carbon concentration, and thus, the LDPE domains should appear as the brightest area in the images. Oxygen predominantly contains in PE-GMA and DGEBA phases hence the oxygen distribution images should reveal the location of their phases. The oxygen distribution images shown are unfortunately noisy and not clear because of the low concentration of the element as compared to sulphur and carbon. Also, the specimen thickness may not be enough thin to create high quality elemental distribution images. It can be mentioned, however, that the PE-GMA and DGEBA phases are not necessary be located at the interfaces between the PPS matrix and the LDPE domains to encapsulate the LDPE domains. Careful observation of the domains in the carbon and the oxygen distribution images reveals that the areas appears as relatively darker in the carbon distribution images give bright contrast in the oxygen distribution images (indicated by arrows in Figure 5). This indicates that the PE-GMA and DGEBA phases do not encapsulate the LDPE domains but stack to the LDPEgMA phase.

To make a clear discussion in terms of the location of the PE-GMA and the DGEBA phases, EELS was performed to detect oxygen core loss peaks in selected regions in the images. A circular area with a diameter of 150 nm was selected, and spectra were taken from those regions. Figure 6 shows the carbon distribution image of the ternary blend of PPS/LDPEgMA/DGEBA (85/10/5) together with EEL-spectra in the range from 480 to 600 eV from the selected regions shown in the image. The spectra from a domain show O K-edge clearly at 530 eV, and also quite a weak O K-edge is detectable even in the spectrum from the PPS matrix. The existence of oxygen in PPS may be due to the curing process during the production of PPS to increase its molecular weight.[15] The two spectra from the different regions in a domain exhibit clear O K-edges with the differences in the intensity of the peaks. The region which gives darker contrast in the carbon distribution image gives stronger core loss peak of oxygen than that from the brighter region. This suggests that the concentration of oxygen is higher in the region which involves the area giving darker contrast in the carbon distribution image. The same result has been obtained in the EELS study in the ternary blends of PPS/LDPEgMA/PE-GMA. Thus, EELS study supports the fact that the PE-GMA and DGEBA phases are not encapsulating the LDPE domains but the two phases are stuck together.

Figure 7 is a zero-loss image, which is formed by elastic scattered and non-scattered electrons, of the ternary blend of PPS/LDPEgMA/PE-MMA (85/10/5) together with EEL-spectra in the range from 500 to 600 eV taken from the regions assigned in the photograph. The spectrum from a relatively larger domain shows no O K-edge, whereas the spectrum from a smaller domain shows the O K-edge at 535 eV. This indicates that the LDPEgMA and the PE-MMA domains are dispersed separately in the PPS matrix. Therefore, PE-MMA does not work as a coupling agent, and consequently, the domain size of LDPEgMA cannot be reduced by the addition of PE-MMA.

There is still no direct evidence of the reaction of PPS against the glycidyl functional materials. However, the above results strongly indicate that PE-GMA and DGEBA work as coupling agents for the PPS matrix and the LDPEgMA domains to improve the dispersion the LDPEgMA phase.

PPS has simple units synthesized from sodium sulfide (Na_2S) and *p*-dichlorobenzene, hence, there seems to be no possibility of the reaction against glycidyl functional materials. The end groups are though to be the candidates of reaction sites; unfortunately, the high insolubility of PPS has precluded the end group identification of this polymer by conventional techniques. Very few publications have described the identification of PPS endgroup chemistry due to analytical difficulties. The polymerization of PPS is carried out with a slight excess of aryl chloride species to avoid conditions leading to polymer degradation. This leads to the expectation that residual aryl chlorides will comprise predominated PPS endgroups. The other candidates for the endgroups of PPS are aryl mercaptide endgroups that are generated after the conversion of sodium thiolate groups treated by an acid. Aryl mercaptide endgroups are expected only when the polymerization does not run to completion. However, even if an endcapping agent was used to ob-

Table III. Tribological properties

Formulation by weight		Coefficient of friction	Wear rate $mm^2 N^{-1} m^{-1}$
PPS/LDPEgMA	90/10	0.20	8.16E-07
PPS/LDPE/E-GMA	89/10/1	0.20	7.34E-07
	85/10/5	0.25	8.97E-07
PPS/LDPE/E-MMA	89/10/1	0.20	1.22E-06
	85/10/5	0.21	1.73E-06
PPS/LDPE/epoxy	89/10/1	0.20	1.12E-06
	85/10/5	0.22	1.26E-06
PPS/PE-GMA	90/10	0.31	1.36E-05
PPS/PE-MMA	90/10	0.72	1.61E-05
PPS/DGEBA	90/10	0.61	5.33E-05
PPS	—	0.80	7.14E-05
MAH-LDPE	—	0.50	1.53E-03

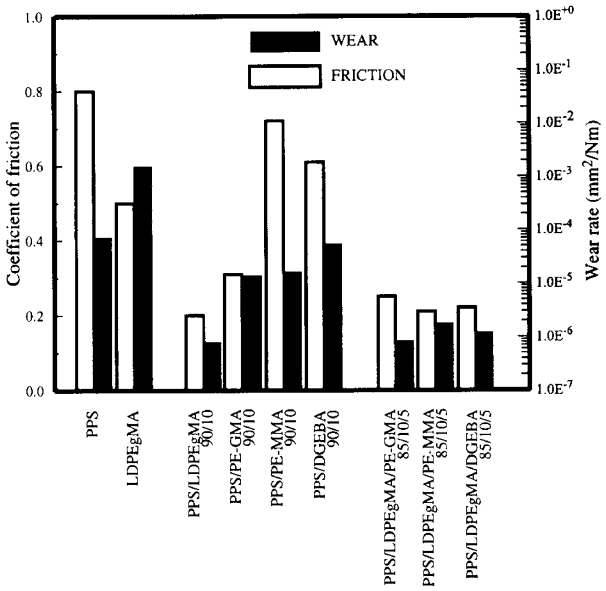

Figure 8. Typical tribological properties obtained in this study.

tain the PPS terminated predominantly by chloro groups, chloro and mercapto endgroups co-existed at certain ratios.[16] Wade *et al.* reported the endgroup characterization of PPS by high temperature MNR,[17] and Reents and Kaplan reported the endgroups of extracted oligomers of PPS by mass mass spectral studies.[18] And then, Risch *et al.* summarized their results.[19] Indeed, aryl chloride endgroups was observed, but mercapt end groups were not detected by their methods. As mentioned by Risch *et al.*, this may be due to their derivatization of the samples. Owing to the different possible mechanisms for termination of the polymerization of PPS, numerous endgroup species are present, such as amino, *N*-alkylamino, and carboxylic acid endgroups. The sources of those species are assumed to be the solvent used for polymerization, *N*-methyl-2-pyrrolidone. Among those detected endgroup species, mercaptide, animes, and carboxylic acid have capability of the reaction to glycidyl functional groups. But the anime endgroups should be excluded as reactive endgroups in our case. If amine endgroups exist in the PPS used in our study, they should directly react to MA grafted on LDPE. As mentioned above, there is no evidence for the reactivity in the binary blend of PPS/LDPEgMA.

It is generally recognized that premade or reactively *in situ* formed block or graft copolymers are generally assumed to prefer to span the interface, resulting in the reduction of the dispersed particle size and the narrow size distribution. In our case, however, the sufficient particle size reduction was achieved although the reactive polymers do not lie on the interface completely. It has been commonly recognized that the main contribution of the premade or reactively formed copolymers is a suppression of coalescence, and not a reduction of interfacial tension.[20] It is, hence, speculated that the glycidyl functional polymers couple the LDPE domains and the PPS matrix, and then, can contribute to the steric hindrance against the coalescence during the melt blending.

The properties of the blends are shown in the following sections, and they will also support the morphological features discussed here.

Tribology

The tribological properties obtained in this study are collected in Table III, and some of their results are shown in Figure 8. Both coefficient of friction and wear rate are significantly decreased by the incorporation of 10 wt% of LDPEgMA into PPS. It is noticeable that the both PPS and LDPEgMA pure homopolymers exhibit poor tribological properties, whereas the blends of these polymers show excellent properties. Especially, wear rate is drastically decreased about the two orders of magnitude. This means that the blends of PPS/LDPE provide the synergistic combination in terms of the tribological properties. Moreover, the ternary blends of PPS/LDPEgMA/PE-GMA, PPS/LDPEgMA/PE-MMA, and PPS/LDPEgMA/DGEBA show the good tribological properties as achieved in the binary blend of PPS/LDPE (90/10). This indicates that the tribological properties are influenced neither by the state of dispersion of the LDPE domains nor by interfacial adhesion between the PPS and the LDPE phases. The tribological properties of the binary blends of PPS/PE-GMA, PPS/PE-MMA, and PPS/DGEBA, on the other hand, are not so much good as the binary blend of PPS/LDPE. Especially, the wear rates of those binary blends are much higher than that of the PPS/LDPEgMA binary blend. As shown in Figure 2, the domain size of PE-GMA, PE-MMA and DGEBA are much smaller than that of the PPS/LDPEgMA binary blends. And also, the interfacial adhesion of the blends of PPS/PE-GMA and PPS/DGEBA are assumed to be stronger than that of the blend of the simple PPS/LDPE blend because of the interfacial chemical reaction between PPS and glycidyl functional materials. This implies that the tribological properties depend on the nature of the chemical structures of the dispersed polymers rather than on the state of their dispersion.

The analogous results regarding the effect of LDPE on the tribological properties have been reported in the blends of polyoxymethylene/LDPE[21] and polyamides/LDPE.[22] Those works suggested that the effect of the addition of LDPE on tribological properties is due to the formation of a thin transferred film by LDPE onto the steel, which works as a lubricating film between the polymer and the steel. It has been known that the tribological properties are greatly affected by the mechanical and thermal properties, and crystallinities originated

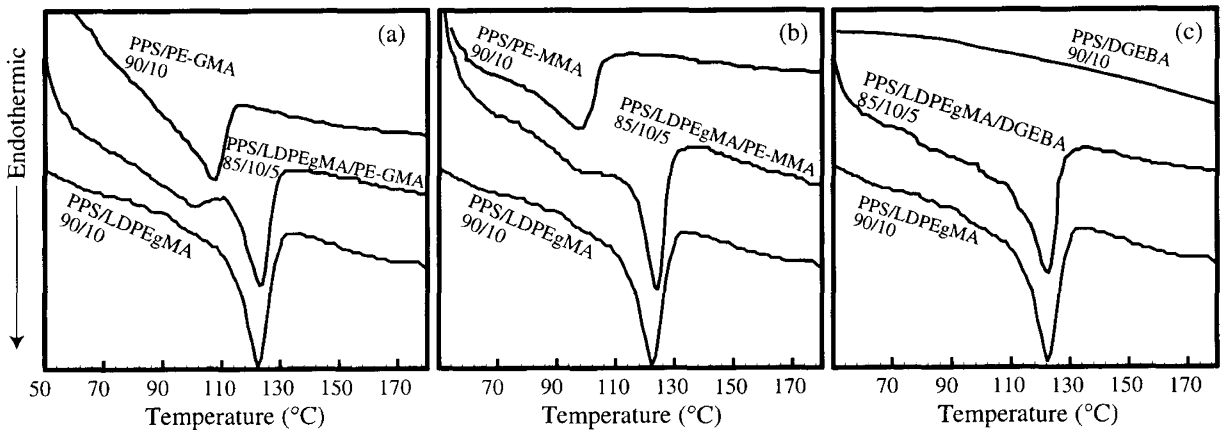

Figure 9. DSC heating traces of the binary and the ternary blends.

from their chemical structures.[23] In the sliding friction, the friction shear and the resultant friction heat result in the deformation and molecular orientation in frictional surfaces of polymers. The differences of the tribological properties among the binary blends, mentioned above, may be derived from the nature of the dispersed polymers, *i.e.*, LDPEgMA, PE-GMA, PE-MMA, and DGEBA.

Figure 9 shows the DSC heating traces of the binary and ternary blends. From the comparison of the binary blend of PPS/LDPEgMA with PPS/PE-GMA (Figure 9a), and with PPS/PE-MMA (Figure 9b), it is revealed that the melting temperatures of PE-GMA and PE-MMA are lower than that of LDPEgMA. This means that the copolymerization of GMA or MMA with ethylene changes the crystalline structure of LDPE to lower the melting temperatures. It was reported that the materials with high molecular symmetry and with high degree of crystallization give lower coefficient of friction.[24] High density polyethylene (HDPE), thus, shows better tribological properties than LDPE.[22] In our case, the reduction of the molecular symmetry and thermal resistance of the crystalline structures, which is caused by the incorporation of GMA or MMA into PE, may be a reason for the reduction of the desirable effect on the tribological properties of the blends. DGEBA, on the other hand, has no crystalline structure as shown in Figure 9c; therefore, both coefficient of friction and wear rate of PPS cannot be improved satisfactory.

The ternary blends of PPS/LDPEgMA/PE-GMA, PPS/LDPEgMA/PE-MMA, and PPS/LDPEgMA/DGEBA, on the other hand, exhibit good tribological properties as well as the PPS/LDPEgMA binary blend despite the addition of the materials that have the unfavorable effect on the tribological properties. The maintaining of the desirable tribological properties in the ternary blends is assumed to come from their morphological features as discussed in the previous section. It was revealed that the glycidyl functional materials and LDPE phases co-exist to be stuck together in the PPS matrix due to their coupling reaction between PPS and LDPEgMA. Suppose that the glycidyl functional materials encapsulate the LDPE domains completely, the poor tribological properties of the binary blends would appear in the ternary blends.

As shown in Figure 9, the melting temperature of LDPEgMA is not influenced by the addition of PE-GMA, PE-MMA, or DGEBA. There appear the two peaks on the DSC traces of the ternary blends as shown in Figure 9a and 9b, which are corresponded to the melting points of LDPEgMA and PE-GMA, and LDPEgMA and PE-MMA, respectively. This fact indicates that the crystalline structure of LDPEgMA is not influenced by the addition of the third components. The LDPEgMA phase should be appear on the surface of specimens by taking the "stuck phase formation" where the LDPEgMA and the glycidyl functional material phases are stuck together, and is in contact with the steel during the tribological test. Therefore, the good tribological properties can be maintained even though the third component that has unfavorable effect on the tribological properties is added to the PPS/LDPE blend.

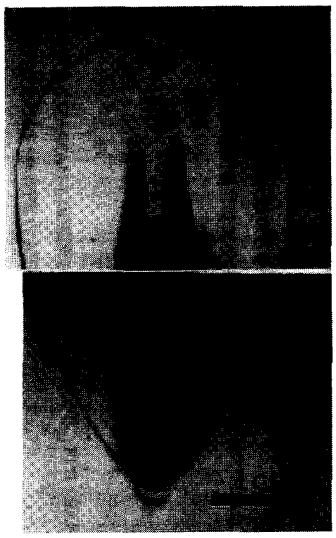

Figure 10. A typical example of MD on the mold surface.

Mold Deposition

The simple blend of PPS/LDPEgMA (90/10) generates deposition on the mold surface during the cyclic operation of injection molding as shown in Figure 10. A mold with a tear-drop shaped cavity was used for the inspection of the MD, and the MD appeared after 5 shots of the injection in the binary blend of PPS/LDPEgMA (90/10). This is a serious problem that rises difficulty in the ejec-

Table IV. Mechanical properties

Formulation		Impact strength	Tensile strength	Elongation at break	Bending strength	Bending modulus	HDT
by weight		J m^{-1}	MPA	%	MPa	GPa	℃
PPS/LDPEgMA	90/10	26	71	3.9	113	3.2	111
PPS/LDPE/E-GMA	89/10/1	38	71	4.5	107	2.9	110
	85/10/5	52	64	5.5	96	2.6	108
PPS/LDPE/E-MMA	89/10/1	24	65	3.2	108	2.9	110
	85/10/5	28	65	3.9	101	2.8	108
PPS/LDPE/epoxy	89/10/1	25	66	3.4	111	3.0	110
	85/10/5	31	66	3.3	111	3.0	107
PPS	—	23	74	3.1	123	2.9	114
MAH-LDPE	—	—	14	336	8	0.2	—

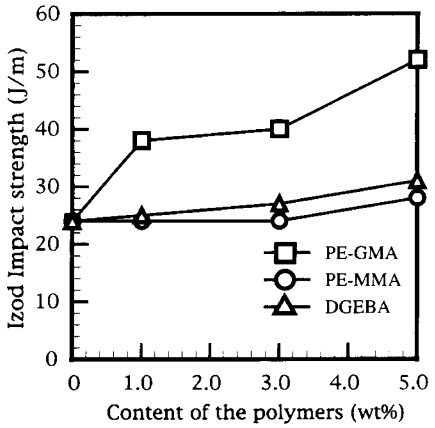

Figure 11. Notched izod impact strength as a function of the concentration of PE-GMA (□), PE-MMA (○), and DGEBA (△). The LDPEgMA content is fixed at 10 wt%, and the contents of those three materials are varied from 1 to 5 wt%.

tion of molded articles and also causes poor surface appearance of them. Taking into account the fact that pure PPS causes no such problem, it is no doubt that the deposition is caused by LDPEgMA. Because PPS exhibits the high melting temperature at 280℃, the mold temperature has to be enough high at 120℃ for sufficient filling of the material into the mold to produce the molded articles without voids and broken off part. However, this would cause the insufficient cooling and solidification of the molten LDPEgMA, and then it would be deposited on the mold surface. To overcome this problem will lead to the improvement of moldability and productivity, and will establish their practical applications.

It was found that introduction of the chemical reaction into the blends of PPS/LDPE can prevent the occurrence of the MD. That is, the addition of 1 wt% of PE-GMA or DGEBA to the PPS/LDPE (90/10) blend prevented the MD even after more than 50 shots of the injection, whereas the addition of PE-MMA could not prevent this unfavorable phenomenon. It is therefore suggested that the coupling reaction between the PPS matrix and the LDPE domains by the glycidyl functional materials can inhibit the deposition of LDPE onto the mold surface, and then prevent the MD in the process of injection molding.

Mechanical Properties

Figure 11 shows the izod impact strength as a function of the concentration of PE-GMA, PE-MMA, and DGEBA in the ternary blends, where the LDPEgMA content is fixed at 10 wt% and the content of those three materials are varied from 1 to 5 wt%. The impact strength of the ternary blends of PPS/LDPEgMA/PE-GMA is increased as an increase of the amount of PE-GMA, whereas the other two blend series show no improvement of the impact strength. As mentioned in the previous section, the ternary blends of PPS/LDPEgMA/PE-GMA and PPS/LDPEgMA/DGEBA exhibit the similar morphologies where the two dispersed phases are stuck together, and the PPS/LDPEgMA/DGEBA blends attain the finer dispersion than the PPS/LDPEgMA/PE-GMA ternary blends. Even though the PPS/LDPEgMA/DGEBA blends attain the finest dispersion, they show no improvement of the impact strength. This distinct difference in terms of the effect on the impact strength is assumed to be due to the defference of the physical characteristics of PE-GMA and DGEBA. That is, DGEBA is a brittle material with relatively low molecular weight, whereas PE-GMA is a ductile crystalline polymer. Hence, PE-GMA contributes to the enhancement of the impact strength, whereas DGEBA does not. The ternary blends of PPS/LDPEgMA/PE-MMA, on the other hand, show the morphologies where the two phases are dispersed separately in the PPS matrix, and the LDPE domain size cannot be reduced as shown in Figure 3, hence the no improvement of the impact strength is achieved.

Table V. Summary and comparison of the properties evaluated in this study

Blend system	Tribology	MD	Impact strength
PPS	Poor	Not occur	Poor
PPS/LDPE	Good	Occur	Poor
PPS/LDPE/PE-GMA	Good	Not occur	Good
PPS/LDPE/PE-MMA	Good	Occur	Poor
PPS/LDPE/DGEBA	Good	Not occur	Poor

Other mechanical properties evaluated in this study are collected in Table IV. Comparing to the pure PPS, the blends show the slight reductions in tensile and bending properties, and also in HDT that refers to the thermal resistance of materials. However, these slight reductions will be within the acceptance for practical applications of these materials.

CONCLUSION

The summary and comparison of the properties evaluated in this study is shown in Table V. Blending of LDPEgMA improves the tribological properties of PPS dramatically, however, it give rise to the MD in the proc-

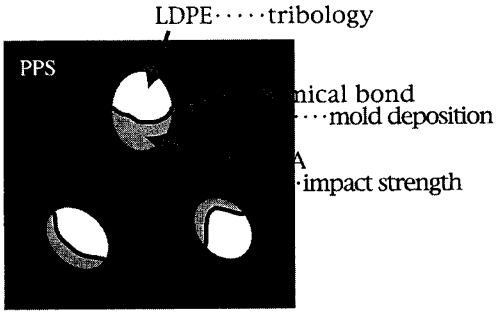

Figure 12. The illustration representing the phase formation achieved in the ternary blends of PPS/LDPEgMA/PE-GMA and explaining the role of the each phases on the specific balanced properties as a result of the synchronization of the three phases.

ess of injection molding. The incorporation of glycidyl functional materials, *i.e.*, PE-GMA or DGEBA, into the PPS/LDPEgMA blends effectively solves this undesirable problem. Moreover, PE-GMA enhances the impact strength as an increase of its content up to 5 wt%. Therefore, the ternary blends of PPS/LDPE/PE-GMA can offer useful materials exhibiting well balanced combination of the properties. It is speculated that the properties thus achieved are owing to the synchronization of the three phases as shown in Figure 12 : The LDPE phase contributes to the improvement of the tribological properties, the coupling reaction between PPS and LDPE by PE-GMA can prevent the MD, and PE-GMA works as an impact modifier.

The synergistic improvement of the tribological properties by blending of PPS and LDPE is an interesting phenomenon, and the detail mechanism has not been obvious. We will investigate this mechanism in the near future.

REFERENCES

1. T. Inoue, M. Okamoto, and M. Yanagi, JP Patent, 58-154757 (1983).
2. M. Inoue, K. Asai, and Y. Suzuku, JP Patent, 62-151461 (1987).
3. N. Nonaka and T. Nitou, JP Patent, 1-198664 (1989).
4. C. M. Chen, H. R. Lee, S. Y. Wu, C. P. Chen, and H. C. Kao, *Anuu. Tech. Conf.*, 2002 (1994).
5. C. M. Chen, H. R. Lee, S. Y. Wu, C. P. Chen, and H. C. Kao, *Anuu. Tech. Conf.*, 2007 (1994).
6. J. Masamoto and K. Kubo, *Polym. Eng. Sci.*, **36**, 265 (1996).
7. J. Choi, S. Lim, J. Kim, and C. R. Choe, *Polymer*, **38**, 4401 (1997).
8. S. Lee and B. C. Chun, *Polymer*, **39**, 6441 (1998).
9. D. R. Fahey, H. D. Hensley, C. E. Ash, and D. R. Senn, *Macromolecules*, **30**, 387 (1997).
10. L. A. Utracki, in "Commercial Polymer Blends", Chapman & Hall, London, 1998, p 428.
11. S. Horiuchi, K. Yase, T. Kitano, N. Higashida, and T. Ougizawa, *Polym. J.*, **29**, 380 (1997).
12. S. Horiuchi, T. Hanada, K. Yase, and T. Ougizawa, *Macromolecules*, **32**, 1312 (1999).
13. L. Reimer, in "Energy-Filtering Transmission Electron Microscopy", L. Reimer, Ed., Springer, Heidelberg, 1995, p 383.
14. R. F. Egerton and R. D. Leapman, in "Energy-Filtering Transmission Electron Microscopy", L. Reimer, Ed., Springer, Heidelberg, 1995, p 271.
15. R. T. Hawkins, *Macromolecules*, **9**, 189 (1976).
16. S. Yang, J. Zhang, Q. Bo, and D. Fang, *J. Appl. Polym. Sci.*, **50**, 1883 (1993).
17. B. Wade, A. S. Abhiraman, S. Wharry, and D. Sutherlin, *J. Polym. Sci., Part B, Polym. Phys.*, **28**, 1233 (1990).
18. W. D. Reents and M. L. Kaplan, *Polymer*, **23**, 310 (1982).
19. B. G. Risch, S. Srinivas, G. L. Wilkes, J. F. Geiel, C. Ash, and M. Hicks, *Polymer*, **37**, 3623 (1996).
20. C. W. Makosko, P. Guegan, A. K. Khandpur, A. Nakayama, P. Marechal, and T. Inoue, *Macromolecules*, **29**, 5590 (1996).
21. S. Takamatsu, T. Kobayashi, T. Komoto, M. Sugiura, and K. Ohara, *Sen-i Gakkaishi*, **50**, 550 (1994).
22. H. Yamane, T. Horiuchi, M. Takahashi, and T. Matsuo, *Key Eng. Mater.*, **137**, 94 (1998).
23. S. Hironaka, *Sekiyu Gakkaishi*, **38**, 137 (1995).
24. Q. Wang, X. Kong, L. Zhu, J. Zhe, and Y. Fan, *J. Appl. Polym. Sci.*, **58**, 903 (1995).